Module FEM-earthquake - Theoretical grounds

1. Basic equations of finite element method accounting for seismic events

The basic equation describing the vibration of a discrete system with N degrees of freedom is written as

$$\mathbf{M}\ddot{\boldsymbol{r}}(t) + \mathbf{C}\dot{\boldsymbol{r}}(t) + \mathbf{K}\boldsymbol{r}(t) = \boldsymbol{F}(t),\tag{1}$$

Equation (1) represents a system of N second order differential equations of motion, where $\dot{r} = \dfrac{\mathrm{d}r}{\mathrm{d}t}$ and $\ddot{r} = \dfrac{\mathrm{d}^2r}{\mathrm{d}t^2}$ represent the velocity and acceleration in the direction of the i-th degree of freedom $(i = 1, \ldots, N)$. In the framework of the finite element method (FEM), the $N \times 1$ vector $\boldsymbol{r}$ stores the components of unknown nodal displacements. The $N \times N$ matrices $\mathbf{M}$, $\mathbf{C}$ and $\mathbf{K}$ stand for the mass, damping and stiffness matrix, respectively. The $N \times 1$ vector $\boldsymbol{F}$ stores the nodal components of the external actions.

The current version of the GEO5 FEM program limits its attention to seismic actions caused by earthquake being represented by the prescribed acceleration of underground longitudinal (pressure P) and transverse (shear S) waves. It is assumed that these waves travel from the bottom boundary of the FEM model towards the terrain surface. The resulting acceleration field in space and time $\ddot{\boldsymbol{u}}(\boldsymbol{x},t)$[1] can be conveniently expressed as a sum of the acceleration prescribed to all nodes of the numerical model $\overline{\boldsymbol{a}}(t)$ and a component $\ddot{\boldsymbol{u}}_R(\boldsymbol{x},t)$ relative to $\overline{\boldsymbol{a}}(t)$.

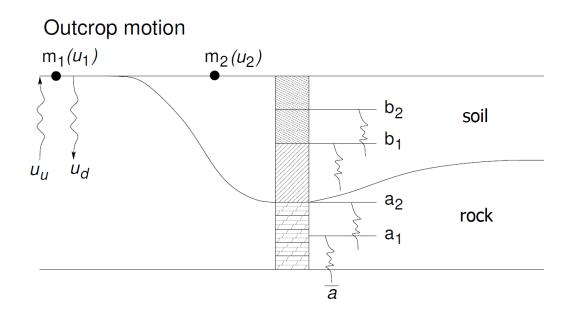$$\ddot{\boldsymbol{u}}(\boldsymbol{x},t) = \overline{\boldsymbol{a}}(t) + \ddot{\boldsymbol{u}}_R(\boldsymbol{x},t).\tag{2}$$

1.1. How to introduce $\overline{\boldsymbol{a}}(t)$ into analysis

The overall displacement at an arbitrary point of the model is equal to the sum of the displacement u_u corresponding to a wave traveling upwards and the displacements u_d associated with a wave traveling downwards, i.e.

$$\boldsymbol{u}(\boldsymbol{x},t) = \boldsymbol{u}_u(\boldsymbol{x},t) + \boldsymbol{u}_d(\boldsymbol{x},t).\tag{3}$$

The seismic motion is typically monitored on the free surface. Such a motion is denoted as the *outcrop motion*, see Fig. 1. To correctly predict the acceleration measured on the terrain (target motion) requires the acceleration $\overline{\boldsymbol{a}}(t)$, prescribed on the bottom boundary, be suitably

---

[1]In the case of 2D analysis the vector $\boldsymbol{u} = \{\mathsf{u}, \mathsf{v}\}$ represents displacements in the direction of coordinate axes x, y.

Obrázek 1: Prescribing acceleration.

adjusted in correspondence to the outcrop motion to account for the type of layers representing the subsoil.

Considering the monitoring point m_1 and the bottom boundary in the bedrock (point a_1) or at the soil-bedrock interface (point a_2) would probably allow us to assume $\overline{\boldsymbol{a}}_{a1,2} \approx \ddot{\boldsymbol{u}}_1$.[2] Providing the bottom boundary is located at points b_1 a b_2, the value of displacement $\boldsymbol{u}_{b1,2}$ may considerably differ from both $\boldsymbol{u}_1$ and $\boldsymbol{u}_2$, i.e. $\overline{\boldsymbol{a}}_{b1,2} \neq \ddot{\boldsymbol{u}}_{1,2}$. For point m_2 one may even expect $\overline{\boldsymbol{a}}_{a1,2} \neq \ddot{\boldsymbol{u}}_2$. To correctly adjust the prescribed acceleration $\overline{\boldsymbol{a}}(t)$ so that the predicted motion approximates the target motion with sufficient accuracy, it is possible to employ the SHAKE software [1]. Further details are available in [2].

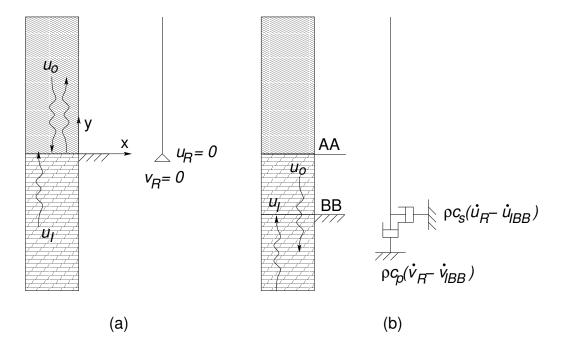*1.2. Definition of boundary conditions on model bottom boundary*

Given the fact that on free surface the amplitude of the upcoming wave equals the one of the reflected wave allows us to write the overall displacement on the terrain surface as twice the displacement of the upcoming wave $\boldsymbol{u}(\boldsymbol{x}, t) = 2\boldsymbol{u}_u(\boldsymbol{x}, t)$. For a general point within a soil body one may adopt Eq. (3). If limiting attention to the bottom boundary this equation receives the form

$$\boldsymbol{u}(\boldsymbol{x}, t)|_{\boldsymbol{x}=\boldsymbol{x}_{BB}} = \boldsymbol{u}_I(\boldsymbol{x}, t)|_{\boldsymbol{x}=\boldsymbol{x}_{BB}} + \boldsymbol{u}_O(\boldsymbol{x}, t)|_{\boldsymbol{x}=\boldsymbol{x}_{BB}}, \tag{4}$$

---

[2]The speed of a seismic wave is proportional to the stiffness of a soil/rock layer through which it propagates. In the rock layer the wave velocity can be of the order of magnitude higher in comparison to the soft soil layer.

where BB denotes the bottom boundary of the numerical model, $\boldsymbol{u}_I$ and $\boldsymbol{u}_O$ represent the incoming wave (wave entering the model) and outgoing wave (wave leaving the model), respectively.

The above relations will be now exploited to define the prescribed acceleration $\bar{\boldsymbol{a}}$ depending on the choice of the boundary conditions specified on the bottom boundary of the numerical model. The GEO5 FEM programs allows the user to define to types of boundary conditions, i.e. fixed and absorbing (quiet) boundary conditions.

Obrázek 2: a) Fixed (kinematic) boundary conditions, b) Absorbing (traction) boundary conditions.

1.2.1. Fixed boundary conditions

The fixed boundary condition can be safely used only in the case when the bottom boundary is found at soft soil/stiff rock interface. Then the incoming wave is "fully" reflected back into the model. Taking into account Eqns. (4) and (2) gives

$$\boldsymbol{u}(\boldsymbol{x},t) = \boldsymbol{u}(t)|_{\boldsymbol{x}=\boldsymbol{x}_{BB}} + \boldsymbol{u}_R(\boldsymbol{x},t), \quad \boldsymbol{u}_R(\boldsymbol{x}=\boldsymbol{x_{BB}},t) = 0, \quad \bar{a}(t) = \ddot{\boldsymbol{u}}(t)_{\boldsymbol{x}=\boldsymbol{x}_{BB}}. \tag{5}$$

As evident from Fig. 2(a) the value of a relative displacement at the bottom boundary BB is equal to zero. Thus the fixed boundary conditions are prescribed along this boundary. The magnitude of the prescribed acceleration $\bar{\boldsymbol{a}}$ thus corresponds to the total motion at BB given by Eq. (3). Recall that for the monitoring point m_1 and the bottom boundary located at point a_2 in Fig. 1 it is possible to consider as the prescribed motion the *outcrop motion* $\bar{\boldsymbol{a}} \approx \ddot{\boldsymbol{u}}_1$.

1.2.2. Absorbing boundary conditions

Consider Fig. 2(b) with the bottom boundary within a layer below the AA interface. In accord with Eqns. (3) and (2) the value of the displacement at an arbitrary point of the layer bounded by the AA and BB interfaces is given by

$$\boldsymbol{u}(\boldsymbol{x},t) = \boldsymbol{u}_I(\boldsymbol{x},t) + \boldsymbol{u}_O(\boldsymbol{x},t) = \boldsymbol{u}_{IBB}(t) + \boldsymbol{u}_R(\boldsymbol{x},t), \tag{6}$$

where $\boldsymbol{u}_{IBB}$ represents the incoming wave at the bottom boundary BB. Because this interface is found within a homogeneous layer the outgoing wave must freely pass this interface. The theoretical model assumes an infinite half-space below this interface. Therefore, the outgoing wave will never return and must be on BB fully damped.

The outgoing wave $\boldsymbol{u}_O$

$$\boldsymbol{u}_O(\boldsymbol{x},t) = \boldsymbol{u}_{IBB}(t) + \boldsymbol{u}_R(\boldsymbol{x},t) - \boldsymbol{u}_I(\boldsymbol{x},t), \tag{7}$$

satisfies on the BB boundary the radiation condition

$$\left\{ \begin{array}{c} \dfrac{\partial u_O(\boldsymbol{x},t)}{\partial x} \\[2mm] \dfrac{\partial v_O(\boldsymbol{x},t)}{\partial y} \end{array} \right\}_{\boldsymbol{x}=\boldsymbol{x}_{BB}} = \begin{bmatrix} \dfrac{1}{c_s} & 0 \\[2mm] 0 & \dfrac{1}{c_p} \end{bmatrix} \left\{ \begin{array}{c} \dfrac{\mathrm{d}u_O(\boldsymbol{x},t)}{\mathrm{d}t} \\[2mm] \dfrac{\mathrm{d}v_O(\boldsymbol{x},t)}{\mathrm{d}t} \end{array} \right\}_{\boldsymbol{x}=\boldsymbol{x}_{BB}} , \tag{8}$$

where c_p a c_s represent the velocities of the propagating P and S waves and are provided by
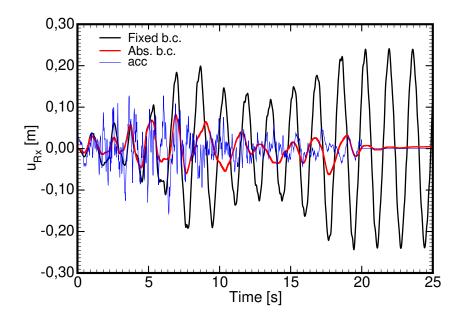
$$c_p = \sqrt{\frac{E_{oed}}{\rho}}, \quad c_s = \sqrt{\frac{G}{\rho}} \tag{9}$$

where ρ, E_{oed}, G are the density, the oedometric modulus and the shear modulus of a given sub-soil layer. With reference to Eqns. (6) and (2) it is, however, necessary to express condition (8) in terms of a relative displacement $\boldsymbol{u}_R$. Approach described in [3] introduces a static boundary condition in the form

$$\left\{ \begin{array}{c} \overline{p}_x = \tau_{xy} \\[2mm] \overline{p}_y = \sigma_y \end{array} \right\}_{\boldsymbol{x}=\boldsymbol{x}_{BB}} = \begin{bmatrix} G & 0 \\[2mm] 0 & E_{oed} \end{bmatrix} \left\{ \begin{array}{c} \dfrac{\partial u_R(\boldsymbol{x},t)}{\partial x} \\[2mm] \dfrac{\partial v_R(\boldsymbol{x},t)}{\partial y} \end{array} \right\}_{\boldsymbol{x}=\boldsymbol{x}_{BB}}$$
$$= \begin{bmatrix} \rho c_s & 0 \\[2mm] 0 & \rho c_p \end{bmatrix} \left\{ \begin{array}{c} \dfrac{\mathrm{d}u_R(\boldsymbol{x},t)}{\mathrm{d}t} - \dfrac{\mathrm{d}u_{IBB}(t)}{\mathrm{d}t} \\[2mm] \dfrac{\mathrm{d}v_R(\boldsymbol{x},t)}{\mathrm{d}t} - \dfrac{\mathrm{d}v_{IBB}(t)}{\mathrm{d}t} \end{array} \right\}_{\boldsymbol{x}=\boldsymbol{x}_{BB}} . \tag{10}$$

A graphical representation of this conditions is seen in Fig. 2(b) as a dashpot with the viscosity ρc_s and ρc_p, respectively. Given Eqns. (6) and (2) the prescribed acceleration reads

$$\overline{\boldsymbol{a}}(t) = \ddot{\boldsymbol{u}}_{IBB}(t). \tag{11}$$

4

Obrázek 3: Comparing response of homogeneous layer generated by fixed and absorbing boundary conditions.

Thus if limiting attention to the monitoring point m_1 in Fig. 1 and the bottom boundary at point a_1 it appears possible to consider the prescribed acceleration to the half of the *outcrop motion*, i.e. $\overline{\boldsymbol{a}} \approx \frac{1}{2}\ddot{\boldsymbol{u}}_1$.
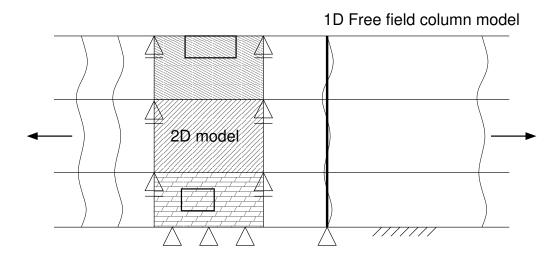
It is also worth noting that the definition of absorbing boundary conditions assumes that layer above the BB boundary behaves linearly elastic. Therefore, the nonlinear response should be allowed for the top layers only.

For illustration, we compare in Fig. 3 the response of a homogeneous 50 m thick layer with either fixed or absorbing boundary conditions subjected to the prescribed horizontal acceleration. Clearly, when the fixed boundary conditions are used the outgoing wave is trapped in the model. Thus for and undamped system the vibration will continue infinitely long. On the other hand, the absorbing boundary will damp the outgoing wave and once the prescribed acceleration ceases the vibration gradually stops. Further details regarding the influence of boundary conditions on the subsoil response can be found in [4, 5].

1.3. Definition of boundary conditions along lateral boundaries

Suppose that both geometrical and material properties of the subsoil do not change in the horizontal direction, see Fig. 4. The response of such a system to the prescribed seismic action will be the same along any vertical section. This corresponds to so called Free field conditions. Such a task can be solved with the help of a one-dimensional (1D) *Free field column* (FF) model.

Solving such a task using a two-dimensional (2D) model truncated in the horizontal direction

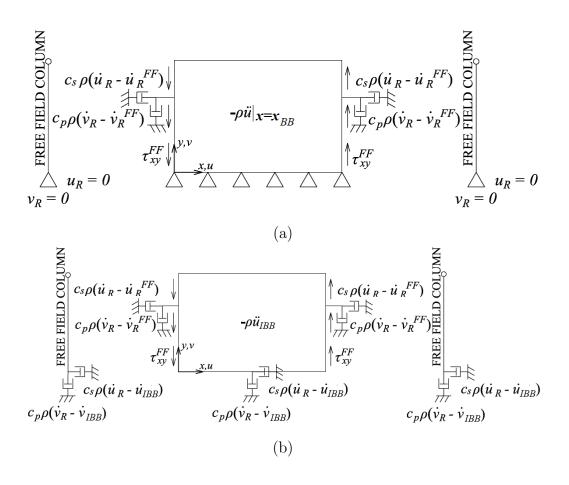Obrázek 4: 2D infinite strip of subsoil and 1D Free field model.

by lateral boundaries (LB), see Fig. 4, calls for introducing suitable boundary conditions along these boundaries to force the response predicted by the 2D model be identical to that of the 1DFF model. In a special case of horizontal motion generating S waves only, the use of standard kinematic conditions in Fig. 4 would be sufficient. However, this is no longer possible when the P and S waves interact. In this general case, the static (traction) boundary condition in terms of the prescribed vertical tractions corresponding to the shear stress τ_{xy}^{FF} provided by the 1DFF analysis proved useful, see Fig. 5.

Providing the Free field conditions are disturbed due to, e.g., excavation (Fig. 4), the part of the motion, corresponding to the difference between the real incoming wave and the one produced by the FF analysis, will have to be damped. This is achieved similarly to the absorbing boundary conditions on the BB boundary (Section 1.2) by introducing radiation (static) boundary conditions as displayed in Fig. 5[3]. For more details the interested reader is referred to [3]. A detailed study of the influence of boundary conditions prescribed on lateral boundaries has been performed in [4].

Assuming the fixed boundary conditions and a 2D analysis, Fig. 5(a), yields the resulting form of Eq. (1) as

$$\mathbf{M}\ddot{\boldsymbol{u}}_R + \mathbf{C}^{\mathsf{M}}\dot{\boldsymbol{u}}_R + \boldsymbol{K}\boldsymbol{u}_R + \mathbf{C}^{\mathsf{LB}}\dot{\boldsymbol{u}}_R|_{x=0,L}$$
$$= -\mathbf{M}\ddot{\boldsymbol{u}}_0 - \mathbf{C}^{\mathsf{M}}\dot{\boldsymbol{u}}_0 + \mathbf{C}^{\mathsf{LB}}\dot{\boldsymbol{u}}_R^{FF}|_{x=0,L} - \boldsymbol{R}_\tau|_{x=0} + \boldsymbol{R}_\tau|_{x=L}, \tag{12}$$

---

[3]Waves approaching the LB boundary in a certain angle not equal to 90° will be damped only partially.

6

Obrázek 5: Boundary conditions on lateral boundaries assuming a) fixed and b) absorbing boundary conditions on bottom boundary. 1D Free field column model and 2D model.

where $\boldsymbol{u}_0 = \boldsymbol{u}(\boldsymbol{x_{BB}})$. For absorbing boundary conditions, Fig. 5(b), we get

$$\mathbf{M}\ddot{u}_R + \mathbf{C}^{\mathsf{M}}\dot{u}_R + \boldsymbol{K}\boldsymbol{u}_R + \mathbf{C}^{\mathsf{BB}}\dot{u}_R|_{y=0} + \mathbf{C}^{\mathsf{LB}}\dot{u}_R|_{x=0,L}$$
$$= -\mathbf{M}\ddot{u}_{IBB} - \mathbf{C}^{\mathsf{M}}\dot{u}_{IBB} + \mathbf{C}^{\mathsf{BB}}\dot{u}_{IBB}|_{y=0} + \mathbf{C}^{\mathsf{LB}}\dot{u}_R^{FF}|_{x=0,L} - \boldsymbol{R}_\tau|_{x=0} + \boldsymbol{R}_\tau|_{x=L}. \qquad (13)$$

The damping matrix will thus split into the contribution due to material damping ($\mathbf{C}^{\mathsf{M}}$) and the influence of absorbing boundary conditions along the BB ($\mathbf{C}^{\mathsf{BB}}$) and LB ($\mathbf{C}^{\mathsf{LB}}$) boundaries, respectively. The load vector $\boldsymbol{F}(t)$ corresponds to the action of inertia forces, the fist term on the right hand side of Eqns. (12) and (13).

1.4. Direct integration of equations of motion

To determine unknown displacements $\boldsymbol{r}$ requires integrating Eq. (1) in time[4]. The GEO5 FEM program employs the implicit Newmark method, which gives the following relationship

---

[4]In GEO5 FEM we solve Eq. (12) or (13) for unknown displacements $\boldsymbol{u}_R$

between displacements, velocities, and accelerations at $n + 1$ integration step providing they are known at step n [6, 7]

$$\boldsymbol{r}_{n+1} = \boldsymbol{r}_n + \Delta t \dot{\boldsymbol{r}}_n + \frac{\Delta t^2}{2} \left[(1 - 2\beta) \ddot{\boldsymbol{r}}_n + 2\beta \ddot{\boldsymbol{r}}_{n+1} \right], \tag{14}$$

$$\dot{\boldsymbol{r}}_{n+1} = \dot{\boldsymbol{r}}_n + \Delta t \left[(1 - \gamma) \ddot{\boldsymbol{r}}_n + \gamma \ddot{\boldsymbol{r}}_{n+1} \right], \tag{15}$$

where Δt represents the time step and β, γ the method parameters to specify the displacement and velocity vectors, respectively. In the light of standard incremental solution in static analysis we modify Eqns.(14) and (15) by introducing the increment of the displacement vector $\Delta \boldsymbol{r} = \boldsymbol{r}_{n+1}$ as

$$\ddot{\boldsymbol{r}}_{n+1} = b_1 \Delta \boldsymbol{r} - b_2 \dot{\boldsymbol{r}}_n - b_3 \ddot{\boldsymbol{r}}_n, \tag{16}$$

$$\dot{\boldsymbol{r}}_{n+1} = b_4 \Delta \boldsymbol{r} - b_5 \dot{\boldsymbol{r}}_n - b_6 \ddot{\boldsymbol{r}}_n, \tag{17}$$

$$\boldsymbol{r}_{n+1} = \boldsymbol{r}_n + \Delta \boldsymbol{r}. \tag{18}$$

where parameters $b_1 - b_6$ are provided by

$$\begin{aligned} b_1 &= \frac{1}{\beta \Delta t^2}, & b_2 &= \frac{1}{\beta \Delta t}, & b_3 &= \frac{1 - 2\beta}{2\beta}, \\ b_4 &= \frac{\gamma}{\beta \Delta t}, & b_5 &= \frac{\gamma}{\beta} - 1, & b_3 &= \frac{\gamma - 2\beta}{2\beta} \Delta y. \end{aligned} \tag{19}$$

Adopting the above equations renders the incremental form of Eq. (1)

$$\left(b_1 \mathsf{M} + b_4 \mathsf{C} + \mathsf{K}^k \right) \Delta \boldsymbol{r} = \boldsymbol{F}_{n+1} + \left(b_2 \mathsf{M} + b_5 \mathsf{C} \right) \dot{\boldsymbol{r}}_n + \left(b_3 \mathsf{M} + b_6 \mathsf{C} \right) \ddot{\boldsymbol{r}}_n - \boldsymbol{R}^k, \tag{20}$$

where $\boldsymbol{F}_{n+1}$ represents the loading at $n + 1$ integration step and $\boldsymbol{R}^k \left(\boldsymbol{R}^0 = \boldsymbol{R}_n \right)$ is the vector of internal nodal forces in the k-th iteration of a given step. The parameters β, γ can be chosen such that the method is stable. Providing the stability does not depend on the size of Δt the method is *unconditionally* stable. It then holds [7]

$$2\beta \leq \gamma \leq \frac{1}{2}. \tag{21}$$

One of the most widely used methods is the *average acceleration method* obtained by setting

$$\beta = \frac{1}{4}, \quad \gamma = \frac{1}{2}, \tag{22}$$

This setting is also generally recommended.

Apart from stability, one should also be concerned with the accuracy of integration. In [7] two specific accuracy measures are introduced to address numerical dissipation and dispersion. The

8

measure of numerical dissipation is the algorithmic damping ratio $\bar{\xi} = \xi + \mathrm{AD}$ and the measure of dispersion is the relative period error $RPE = \dfrac{\overline{\mathrm{T}} - \mathrm{T}}{\mathrm{T}}$. The parameter ξ is the material damping ratio, see Section 4), AD represents the amplitude decay attributed to the selected numerical integration scheme, T is the real period of vibration and $\overline{\mathrm{T}}$ is the period associated with the discrete system. Providing $\gamma = \dfrac{1}{2}$, we get AD=0. In such a case, the amplitude decay, if not assuming the absorbing boundary conditions, will be caused by the material damping only (the matrix $\mathbf{C}^{\mathrm{M}}$, e.g. in Eq. (12)) driven by the value of ξ.

However, in the solution of a discrete system it is often desirable to have AD $\neq 0$ to filter out high-frequency modes, which are artifacts of the discretization into finite elements, while keeping good accuracy in the load modes. To that end, the algorithm introduced in [8] and termed the α-method deserves particular attention. This method modifies the original Eq. (20) as

$$\left[b_1 \mathbf{M} + (1 + \alpha) b_4 \mathbf{C} + (1 + \alpha) \mathbf{K}^k \right] \Delta \boldsymbol{r} = \tag{23}$$
$$\boldsymbol{F}_{n+1} + \left[b_2 \mathbf{M} + ((1 + \alpha) b_5 + \alpha) \mathbf{C} \right] \dot{\boldsymbol{r}}_n + \left[b_3 \mathbf{M} + (1 + \alpha) b_6 \mathbf{C} \right] \ddot{\boldsymbol{r}}_n - \boldsymbol{R}^k,$$

where $t_{n+\alpha} = t_{n+1} + \alpha \Delta t$. For $\alpha = 0$ we recover Eq. (20).

For the method to be unconditionally stable and second order accurate requires

$$\alpha \in \left[-\frac{1}{3}, 0 \right], \quad \beta = \frac{1 - \alpha^2}{4}, \quad \gamma = \frac{1 - 2\alpha}{2}. \tag{24}$$

Clearly, increasing α decreases the amount of numerical damping. For $\alpha = 0$ we get $\gamma = \dfrac{1}{2}$, i.e. AD=0.

Both the average acceleration method and α-method are unconditionally stable. The selected integration time step thus determines the accuracy, or vice versa. To a large extent, this is affected by material properties and the type of finite element mesh (type and size of the element, local mesh refinement). Thus in general settings, to define an optimal time step is not an easy task.

For conditionally stable Newmark method ($\gamma \leq \dfrac{1}{2}$, $\beta \leq \gamma$), the time step Δt must comply with following condition [7]

$$\Delta t \leq \Delta t_{crit}, \quad \Delta t_{crit} = \frac{\Omega_{crit}}{\omega_{eq}}, \tag{25}$$

$$\Omega_{crit} = \frac{\xi \left(\gamma - \frac{1}{2} \right) + \left[\frac{\gamma}{2} - \beta + \xi^2 \left(\gamma - \frac{1}{2} \right)^2 \right]^{\frac{1}{2}}}{\frac{\gamma}{2} - \beta}, \tag{26}$$

9

where Ω_{crit} is the critical sampling frequency and ω_{eq} is the maximum natural frequency of the discrete system, which can be bounded by the maximum frequency of individual elements[5]. Perhaps the most widely used unconditionally stable Newmark method is the *central difference scheme* ($\beta = 0$, $\gamma = \frac{1}{2}$ and for $\xi = 0$ is $\Omega_{crit} = 2$). For the diagonal mass and damping matrices, this method is explicit. To minimize the period error it is recommended to combine the diagonal mass matrix (lumped mass matrix) with the central scheme, while the consistent mass matrix should be used with the average acceleration method [7]. Because the GEO5 FEM program assumes the consistent mass matrix for all types of elements, the use of central difference scheme is not recommended.

The list of Δt_{crit} for the 1D linear and quadratic rod elements considering both the lumped and consistent mass matrices is available, e.g. in [7]. Further examples can be found in [9]. The PLAXIS [10] program exploits for triangular higher order elements the estimates of Δt_{crit} presented in [11].

To conclude, point out that in the case of earthquake the maximum time step depends on the acceleration record, which in general assumes sampling in the interval of $\Delta t \in [0.005, 0.01]\,\mathrm{s}$.

2. Solution of eigenvalue problem

The GEO5 FEM program allows for the determination of eigenvalues (natural frequencies) and eigenvectors (mode shapes) of a discrete problem by solving the generalized eigenvalue problem of an undamped system in the form

$$(\mathbf{M} - \lambda_\alpha \mathbf{K})\, \boldsymbol{\phi}_\alpha = \mathbf{0}, \quad \lambda_\alpha = \omega_\alpha^2, \tag{27}$$

where $\boldsymbol{\phi}_\alpha$ is the eigenvector associated with the eigenvalue λ (natural frequency ω_α). During analysis, the eigenvectors are normalized with respect to the mass matrix as
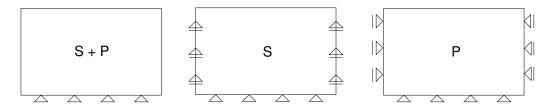
$$\overline{\boldsymbol{\phi}}_\alpha = \frac{\boldsymbol{\phi}_\alpha}{\left[\boldsymbol{\phi}_\alpha^\mathsf{T} \mathbf{M} \boldsymbol{\phi}_\alpha\right]^{\frac{1}{2}}} \qquad \text{unit} \quad \left[\frac{1}{\sqrt{t}}\right]. \tag{28}$$

For the sake of visual presentation, the eigenvectors are further scaled by the maximum total nodal displacement (k-node number, Nn-total number of nodes) as

$$\overline{\overline{\boldsymbol{\phi}}}_\alpha = \frac{\overline{\boldsymbol{\phi}}_\alpha}{A_\alpha^{max}} \;\; [-], \qquad A_\alpha^{max} = \max_{k=1}^{Nn}\left(\sqrt{(\phi_{\alpha,k}^x)^2 + (\phi_{\alpha,k}^y)^2}\right). \tag{29}$$

---

[5]It is seen that for $\gamma = \frac{1}{2}$, the viscous damping has no effect on stability.

The GEO5 FEM program solves Eq.. (27) for the selected number of the lowest eigenvalues using standard method of subspace iteration [6, 7, 12]. To solve this task one may choose either the Jacobi method or the Gram Schmidt orthogonalization method. In each iteration step, the Jacobi method solves the reduced eigenvalue problem. This analysis is, however, very effective and the total number of required global iterations is typically less than when using the Gram Schmidt orthogonalization method. However, the Jacobi method does not guarantee that the first K eigenvalues will always be found.

Obrázek 6: Kinematic boundary conditions available for solving the eigenvalue problem.

When solving the eigenvalue problem the GEO5 FEM program allows the user to consider three types of kinematic boundary conditions, see Fig. 6. The first case (S+P) does not account for a specific vibration mode. On the contrary, the second and the third option makes preference of a horizontal (S) and vertical (P) vibration mode, respectively. Nevertheless, it is recommended to make a visual check prior to selecting the desired vibration mode, e.g. for the calculation of parameters of material damping described in Section 4. An additional hint for choosing the vibration mode might the *Modal participation factor* and *Modal effective mass.*

2.1. Modal participation factor

We limit our attention to 2D plane-strain analysis with no account for rotational degrees of freedom. The modal participation factor $\Gamma_{\alpha,i}$ for mode α in the direction ($i \equiv x$ or $i \equiv y$) is given by

$$\Gamma_{\alpha,i} = \frac{\{\overline{\phi}_\alpha\}^\mathsf{T} [\mathsf{M}] \{\mathsf{l}_i\}}{m_\alpha} \qquad \text{unit } \left[\sqrt{t}\right],\tag{30}$$

and indicates how strongly the motion in the direction of the coordinate axis x, y is represented in the eigenvector $\{\phi_\alpha\}$. The vector $\{\mathsf{l}_i\}$ is the influence vector associated with either the horizontal ($i \equiv x, \{\mathsf{l}_x\}^\mathsf{T} = \{1, 0, 1, 0, \ldots, 1, 0\}$) or vertical ($i \equiv y, \{\mathsf{l}_y\}^\mathsf{T} = \{0, 1, 0, 1, \ldots, 0, 1\}$) component of the vibration. The generalized mass m_α is written as

$$m_\alpha = \{\overline{\phi}_\alpha\}^\mathsf{T} [\mathsf{M}] \{\overline{\phi}_\alpha\} \ [-].\tag{31}$$

11

Because the eigenvectors in the GEO5 FEM program are normalized with respect to the mass matrix, we get $m_\alpha = 1$.

2.2. Modal effective mass

Another parameter representing participation of a given eigenvector in either horizontal or vertical component of the vibration is the modal effective mass

$$m_{\alpha,i} = (\Gamma_{\alpha,i})^2 \, m_\alpha \qquad \text{unit } [t]. \tag{32}$$

This parameter can be adopted to determine the minimum number of eigenvectors to be used in application of modal analysis to solve Eq. (1). It holds that the sum of modal effective masses $m_{\alpha,i}$ of all modes in any particular direction ($i \equiv x$ or $i \equiv y$) is equal to the total mass, except for the mass associated with kinetically constrained degrees of freedom. The program provides the total modal effective mass in either direction as

$$\text{TMEM}_i = \sum_{\alpha=1}^{M} m_{\alpha,i}, \tag{33}$$

where M is the number of adopted (determined) modes. The minimum number of eigenvectors is typically determined such as the TMEM_i value exceeds the 90% of the total mass. If this value is considerably smaller than the total mass, it means that the modes that have a significant participation in that direction have not been extracted.
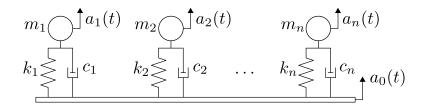
3. Response spectrum - generation of artificial accelerograms

To describe a seismic motion we generally use accelerograms, i.e. the time variation of ground acceleration. In 2D analysis, such a motion considers two components of the acceleration vector. One component serves to describe motion in the horizontal direction, the other one in the vertical direction. The Eurocode 8 (EC8) allows for the description of seismic motion the application of artificial, real or simulated accelerograms.

The real accelerograms follow from the measurements of real earthquakes by seismographic stations installed all over the world. Simulated accelerograms are obtained by simulating both the source of a seismic activity and mechanism of transport of seismic waves. However, the interest of structural engineers is usually shifted towards artificial accelerograms. This is why we address this issue in the next subsections in more details.

3.1. Elastic response spectrum

The elastic response spectrum of an accelerogram is represented by the graph of a function $a(T)$ the value of which is defined as the maximum acceleration of a harmonic oscillator with a single degree of freedom having the natural period T and being exited by this accelerogram. The physical model adopted to compute the response spectrum is plotted in Fig. 7. Each oscillator i with the mass m_i, the spring stiffness k_1, and the coefficient of viscous damping c_i has the natural frequency $\omega_{0,i} = \sqrt{k_i/m_i}$ and the coefficient of proportional damping $\xi_i = c_i/(2\sqrt{m_i k_i})$. Providing its base is exited by the acceleration, the corresponding mass will move with the acceleration $a_i(t)$. The maximum absolute value of $a_i(t)$ represents the value of response spectrum $S_e(a_i)$ plotted as a function of $T_i = 2\pi/\omega_{0,i}$. An example of the design response spectrum appears in Fig. 8.
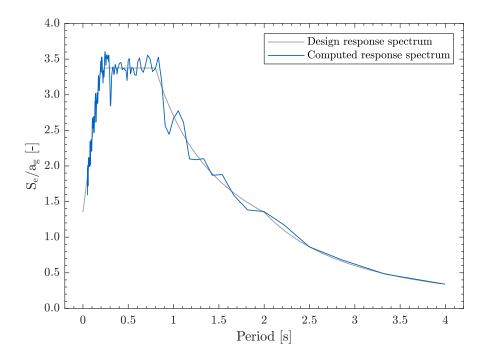

Obrázek 7: Principle of computation of elastic response spectrum: harmonic oscillators with various natural frequencies exited by accelerogram $a_0(t)$ and monitored response $a_i(t)$.

3.2. Artificial accelerograms

An artificial accelerogram has to be generated such as to correspond to the elastic response spectrum with the viscous damping $\xi = 0.05$ defined in the Eurocode 8. This standard further determines the minimum duration of the acceleration and their minimum number used to address the response of a structure to seismic actions.

The algorithm to generate artificial accelerograms is taken from [13] and consists from the following steps:

1. The Fourier spectrum with constant spectral amplitudes and random phase shifts is generated.

2. The Fourier transform is then used to get the corresponding time variation of acceleration.

3. For this accelerogram, the elastic response spectrum of single degree of freedom systems with frequencies corresponding to frequencies used in the Fourier spectrum is computed.
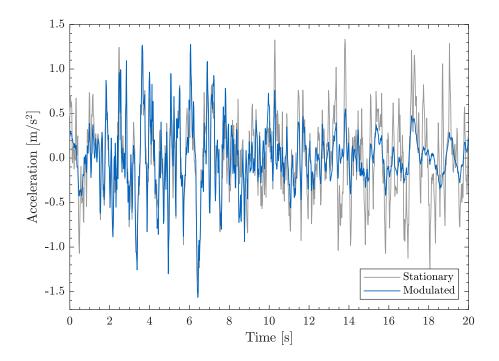
Obrázek 8: Comparing design response spectrum defined by EC8 and response spectrum extracted from generated accelerogram, adopted from [5].

4. The contribution of the design elastic response spectrum specified by EC8 and the contribution due to the generated accelerogram are computed for each frequency.

5. Spectral amplitudes of the original Fourier spectrum are adjusted based on the contributions acquired in the previous step. The phase shifts remain the same.

6. The steps 2–5 are repeated for the adjusted Fourier spectrum until the calculated response spectrum matches the design elastic response spectrum due to EC8 up to an error less than 10 %, see Fig. 8.

The accelerogram obtained from this algorithm complies with the EC8 conditions, but it is stationary and lacks characteristic stages typical of real measured accelerograms, see the stationary distribution in Fig. 9.

For this accelerogram to contain an amplification stage, a region of strong motion, followed by gradual decay it is necessary to multiply the stationary accelerogram by an envelope function $E(t)$ [14]

$$E(t) = at^b e^{-ct}, \tag{34}$$

Obrázek 9: Comparing stationary and non-stationary (modulated) artificial accelerograms, adopted from [5].

with coefficients

$$a = \left(\frac{e}{\varepsilon T_w} \right)^b, \tag{35}$$

$$b = \frac{-\varepsilon \ln \mu}{1 + \varepsilon(\ln \varepsilon - 1)}, \tag{36}$$

$$c = \frac{b}{\varepsilon T_w}. \tag{37}$$

where T_w the specific earthquake duration. The parameter ε determines at what time instant of T_w the envelope function attains its maximum value. The parameter μ determines the reduction factor of the envelope function at time T_w with respect to ts maximum value.

The accelerogram is generated such to get zero velocity and displacement at time T_w, while zero initial velocity and displacement contained already by the stationary accelerogram are retained. The impact of the application of envelope function on the time variation of the generated acceleration is illustrated in Fig. 9, compare stationary and non-stationary accelerograms. Further details regarding the response spectrum and accelerograms in connection to EC8 are available in [15, 16]. For details on the use of envelope function the interested reader is referred to [13].

4. Introducing material damping

The most simple approach to constructing the damping matrix $\mathbf{C}^{\mathsf{M}}$, adopted also in the GEO5 FEM program, is based on the assumption of proportional damping. In such a case it holds

$$\mathbf{\Phi}^{\mathsf{T}}\mathbf{C}^{\mathsf{M}}\mathbf{\Phi} = 2\mathbf{\Omega}^d, \tag{38}$$

where $\mathbf{\Phi}$ is the modal matrix the columns of which are represented by individual eigenvectors of the vibrating system, recall Section 2. The matrix $\mathbf{\Omega}^{\mathbf{d}}$ is diagonal with the components $\omega_i^d = \xi_i\omega_i$, where ω_i^d denotes the damped frequency and ξ_i is the coefficient of proportional damping associated with the natural frequency ω_i. Then, the eigenvectors are orthogonal also to the damping matrix $\mathbf{C}^{\mathsf{M}}$. In case of modal decomposition the solution of Eq. (1) splits into the system of n independent differential equations, where n is the number of used eigenvectors, which considerably simplifies the analysis.

Formulation of proportional damping (38) is very simple, but it assumes the knowledge of the coefficients of proportional damping ξ_i for all the frequencies. This can hardly be achieved in practice. Additional hypothesis allowing for the determination of all ξ_i on the basis of just a few constants is therefore needed. In this regard, it is convenient to consider in most practical applications the Rayleigh damping which assumes the damping matrix $\mathbf{C}^{\mathsf{M}}$ in the form of linear combination of the mass and stiffness matrices as

$$\mathbf{C}^{\mathsf{M}} = \alpha\mathbf{M} + \beta\mathbf{K}, \tag{39}$$

where α, β are the parameters of proportional damping[6]. The fact that the eigenvectors in the GEO5 FEM program are normalized with respect to the mass matrix provides upon multiplying Eq (39) from the left by $\mathbf{\Phi}^{\mathsf{T}}$ and from the right by $\mathbf{\Phi}^{\mathsf{T}}$

$$2\mathbf{\Omega}^d = \alpha\mathbf{I} + \beta\mathbf{\Omega}^2 \longrightarrow 2\omega_i^d = 2\xi_i\omega_i = \alpha + \beta\omega_i^2, \tag{40}$$

where $\mathbf{I}$ is the identity matrix. The spectral matrix $\mathbf{\Omega}$ is similar to $\mathbf{\Omega}^d$ diagonal and collects on the diagonal the squares of natural frequencies.

It is evident from Eq. (40) that to determine parameters α, β it is sufficient to know two eigenfrequencies ω_i and their corresponding coefficients ξ_i. If we accept that both frequencies

---

[6]These parameters should not be confused with the parameters α, β, γ introduced in Section 1.4.

ω_a and ω_b are damped by the same coefficient of proportional damping, i.e. $\xi_a = \xi_b = \xi$, we get

$$\alpha = \frac{2\xi\omega_a\omega_b}{\omega_a + \omega_b}, \qquad \beta = \frac{2\xi}{\omega_a + \omega_b}. \tag{41}$$

However, most often we have at our disposal only one value of the coefficient of proportional damping for the lowest natural frequency ω_1. If we accept the hypothesis that this frequency is damped the least, then using Eq. (40) gives

$$\frac{d\xi}{d\omega_i} = \frac{1}{2}\Big(-\frac{\alpha}{\omega_i^2} + \beta\Big) = 0. \tag{42}$$

Introducing $\omega_i = \omega_1$ into Eq. (42) yields
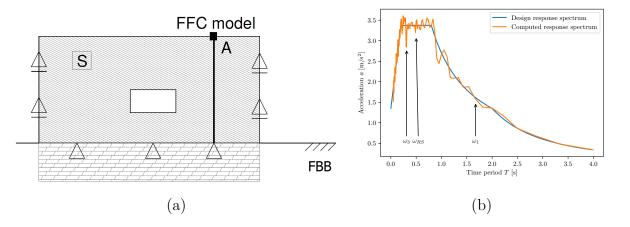
$$\alpha = \omega_1^2\beta. \tag{43}$$

Back substitution for α from Eq. (43) into Eq. (40) finally provides

$$\alpha = \xi_1\omega_1, \qquad \beta = \frac{\xi_1}{\omega_1}. \tag{44}$$

Further details can be found in [6].

4.1. Example of calculating α, β

Details regarding the presented example including the geometry of the numerical model and material properties of individual layers of subsoil are available in [5]. Henceforth, we limit our attention to a brief description of the potential way of calculating the parameters of Rayleigh damping α, β.

Obrázek 10: a) Subsoil model, b) Response spectrum.

Eurocode 8 offers a single values of proportional damping $\xi = 0.05$ (5%) only. The presented example will show, how strongly are individual natural frequencies damped in dependence on

17

the way of calculating the parameters α, β. For illustration, we consider a simple model displyed in Fig. 10(a). The impact of material damping is best evaluated on the basis of fixed boundary conditions on the BB boundary (FBB). To allow for relating the natural frequencies of the system to the prescribed acceleration we shall consider the accelerogram in Fig. 3 generated on the grounds of the design reponse spectrum plotted in Fig. 10(b), recall Section 3.

This accelerogram introduces the horizontal (shear) seismic waves only. Thus to determine the first few natutral frequencies, we considered the kinematic boundary conditons on the lateral boundaries in accordance with Fig. 10(a), recall also Section 2 and Fig. 6. To identify purely shear dominated mode shapes we employed the *Modal participation factor* $\Gamma_{\alpha,x}$.

The following three variants of the calculation of parameters α, β are presented for illustration:

1. The least damped is the first natural frequency. The parameters α, β follow from Eq. (44).

2. The least damped frequecies are found between the first and third[7] natural frequency. The third natural frequency was adopted according to recommendations presented in [10]. The parameters α, β follow from Eq. (41).

3. The least damped frequencies are found between the first and the the most dominant frequency ω_{RS} of the design response spectrum, see Fig. 10(b). The parameters α, β follow from Eq. (41).

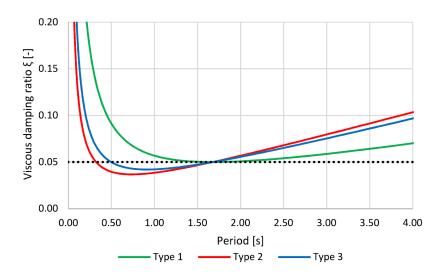Tabulka 1: Parameters of Rayleigh damping for $\xi = 5\%$, adopted from 1

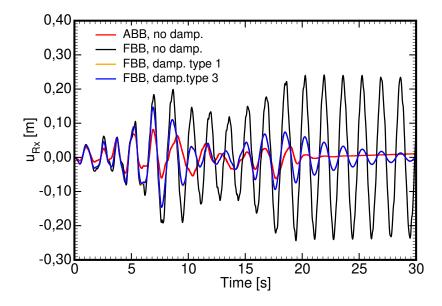| Damping	ω	α	β
Typ 1	ω_1	0.1875	0.0133
Typ 2	$\omega_1 + \omega_3$	0.3143	0.0043
Typ 3	$\omega_1 + \omega_{RS}$	0.2888	0.0061

The resulting values of natural frequencies and parameters α, β are summarized in Table 1. A graphical representation of the amount of damping is provided in Fig. 11. Clearly, only the chosen frequncies are damped with $\xi = 5\%$. Apart from identifying the domain of the least damped frequecies we also absored that particularly high frequecies of the design spectrum are damped the most[8].

---

[7]More specifically, the third frequency from the list of purely shear mode shapes.
[8]The abscissa represents natural periods $T = \frac{2\pi}{\omega}$.

18

Obrázek 11: Proportional damping ratio as a function natural period.

Obrázek 12: Comparing response of homogeneous layer assuming fixed and absorbing boundary conditions to evaluate influnce of material damping.

Finally, to judge the influence of material damping we compare the influnce of fixed and absorbing (ABB) bounary conditions on the response of a homogeneous layer exited by the horizontal seismic waves generated from the design response spectrum in Fig. 10(b). For simplicity, we consider the *Free field column* analysis depicted in Fig. 10(a). The resulting distributions of the relative horizontal displacement at point A are seen in Fig. 12. The impact of material damping is evident and in the case of FBB conditions it repersents the only way how to bring he vibrating system to rest once the applied acceleration ceases. For ABB conditions, the material damping does not play a significant role.

5. Solution process

It is clear from the previous text that earthquake analysis requires a certain sequence of calculations. In particular:

1. **Static analysis** in a given stage to get the initial stress state prior to application of dynamic load (prescribed acceleration).

2. **Solution of the eigenvalue problem to acquire natural frequencies and mode shapes**. The program determines the first M eigenfrequencies $\omega_1 < \omega_2 < \ldots < \omega_M$, where M the required number set by the user. Depending on the solution setting it may happen that not all requested eigenfrequencies were extracted or some of them were missed. When employing the Jacobi method the program searches for more frequencies than requested so that the number frequencies found typically exceeds the number specified by the user. The program offers a table collecting not only all converged frequencies but also the ones found with the error larger than the one specified in the solution setting. The maximum error associated with the highest frequency is provided. The table also lists for each eigenfrequency the *Modal participation factor* and *Modal effective mass* identifying which of the basic vibration modes (vibration either horizontal or vertical directions) prevails in the given eigenvector. A visual check is available by animating the particular eigenvector. The extracted eigenfrequencies can be used to determine the parameters of α, β of the Rayleigh damping when specifying the coefficient of proportional damping ξ in the material setting. The solution process can be terminated after completing the eigenvalue analysis to verify, either visually or numerically, the expected range of frequencies used in the calculation of α, β, recall Section 4.

3. **Free field column analysis**. The Free field column analysis provides the time variation of traction boundary conditions prescribed on lateral boundaries of the computational model, see Section 1.3. On both boundaries, the analysis is carried out simultaneously. The material models in individual layers, boundary conditions on the BB boundary, the prescribed acceleration, and the initial time step comply with the 2D analysis. The results of this analysis cannot be visualized.

4. **Two-dimensional earthquake analysis pertinent to given calculation stage**. The analysis provides a time variation of all quantities. These can be presented in an arbitrary time step, visualized step by step or animated.

Literature

[1] P. Schnabel, J. Lysmer, B. Seed, SHAKE, a computer program for earthquake response analysis of horizontally layered sites, Tech. rep., Earthquake Engineering Re-search Center, University of California, Berkeley. Report No. EERC 72-12 (1972).

[2] L. Mejia, E. Dawson, Earthquake deconvolution for FLAC, in: H. . Varona (Ed.), 4th International FLAC Symposium on Numerical Modeling in Geomechanics, 2006, pp. 4–10.

[3] O. C. Zienkiewicz, N. Bicanic, F. Q. Shen, Generalized Smith boundary – – a transmitting boundary for dynamic computation, Institute for Numerical Methods in Engineering, University College of Swansea 207.

[4] V. Pavelcová, T. Poklopová, T. Janda, M. Šejnoha, The influence of boundary conditions on the response of underground structures subjected to earthquake, Acta Polytechnica CTU Proceedings 15 (2018) 74–80.

[5] V. Pavelcová, T. Poklopová, T. Janda, M. Šejnoha, Influence of material damping on the response of underground structures subjected to earthquake, Acta Polytechnica CTU Proceedings 26 (2020) 64–70.

[6] Z. Bittnar, P. Řeřicha, Metoda konečných prvků v dynamice konstrukcí, SNTL, 1981.

[7] T. Hughes, The Finite Eelement Method: Linear Static and Dynamic Finite Element Analysis, Prentice Hall, INC., Englewood Clifts, New Jersey 07632, 1987.

[8] H. Hilber, T. Hughes, R. Taylor, Improved numerical dissipation for time integration algorithms in structural dynamics, Earthquake Engineering and Structural Dynamics 5.

[9] T. Belytschko, An Overview of Semidiscretization and Time Integration Procedures, in: T. B. . T. Hughes (Ed.), Computational Methods for Transient Analysis, 1983, pp. 1–65.

[10] R. Brinkgreve, E. Engin, W. Swolfs, Plaxis 2D manual, http://www.plaxis.nl (*Rotterdam, Netherlands, Balkema*, 2017).

[11] O. Pal, Modélisation du comportement dynamique des ouvrages grâce á des éléments finis de haute précision, Ph.D. thesis, L'université Joseph Fourier - Grenoble I. (1998).

[12] Z. Bittnar, J. Šejnoha, Numerical methods in structural engineering, ASCE Press, 1996.

[13] A. Kumar, Software for generation of spectrum compatible time history, in: Proceedings of 13th World Conference on Earthquake Engineering, 2004, pp. 1–6.

[14] D. M. Boore, Stochastic simulation of high-frequency ground motions based on seismological models of the radiated spectra, Bulletin of the Seismological Society of America 73 (6A) (1983) 1865–1894.

[15] J. Máca, K. Pohl, Seizmická odolnost stavebních konstrukcí, https://docplayer.cz/15128735-Seizmicka-odolnost-stavebnich-konstrukci.html, [Online; cit. 2019-11-03] (Workshop 2005 – VZ "Udržitelná výstavba").

[16] L. Janošková, Dynamická analýza konstrukce zatížené seismickým zatížením, diplomová práce, *Vysoké učení technické v Brně* (2013).